Science of the Total Environment 873 (2023) 162330

Contents lists available at ScienceDirect

Science of the Total Environment

journal homepage: www.elsevier.com/locate/scitotenv

Coal-source acid mine drainage reduced the soil multidrug-dominated antibiotic resistome but increased the heavy metal(loid) resistome and energy production-related metabolism

Qiang Huang [a], Zhenghua Liu [b,e], Yuan Guo [a], Bao Li [a,c], Zhenni Yang [b], Xiaoling Liu [a], Jianmei Ni [a], Xiutong Li [b,c], Xi Zhang [b,c], Nan Zhou [b], Huaqun Yin [e], Chengying Jiang [b,c,1], Likai Hao [a,c,d,*,1]

[a] State Key Laboratory of Environmental Geochemistry, Institute of Geochemistry, Chinese Academy of Sciences, Guiyang 550081, PR China
[b] State Key Laboratory of Microbial Resources, Institute of Microbiology, Chinese Academy of Sciences, Beijing 100101, PR China
[c] University of Chinese Academy of Sciences, Beijing 100049, PR China
[d] CAS Center for Excellence in Quaternary Science and Global Change, Xi'an 710061, PR China
[e] School of Minerals Processing and Bioengineering, Key Laboratory of Biometallurgy of Ministry of Education, Central South University, Changsha 410083, PR China

HIGHLIGHTS

- AMD contamination decreased the relative abundance of multidrug-dominated ARGs.
- AMD contamination increased the relative abundance of MRGs and MGEs.
- Both the microbial community and MGEs drove the MRG dynamic.
- AMD contamination increased energy production-related metabolism.

GRAPHICAL ABSTRACT

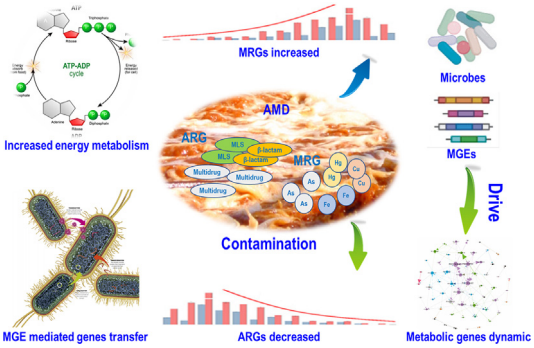

ARTICLE INFO

Editor: Filip M.G. Tack

Keywords:
Metagenome
Resistome
Mobile gene elements
Energy-production metabolism
Acid mine drainage

ABSTRACT

A recent global scale study found that mining-impacted environments have multi-antibiotic resistance gene (ARG)-dominated resistomes with an abundance similar to urban sewage but much higher than freshwater sediment. These findings raised concern that mining may increase the risk of ARG environmental proliferation. The current study assessed how typical multimetal(loid)-enriched coal-source acid mine drainage (AMD) contamination affects soil resistomes by comparing with background soils unaffected by AMD. Both contaminated and background soils have multidrug-dominated antibiotic resistomes attributed to the acidic environment. AMD-contaminated soils had a lower relative abundance of ARGs (47.45 ± 23.34 ×/Gb) than background soils (85.47 ± 19.71 ×/Gb) but held high-level heavy metal(loid) resistance genes (MRGs, 133.29 ± 29.36 ×/Gb) and transposase- and insertion sequence-dominated mobile genetic elements (MGEs, 188.51 ± 21.81 ×/Gb), which was 56.26 % and 412.12 % higher than background soils, respectively.

Procrustes analysis showed that the microbial community and MGEs exerted more influence on driving heavy metal (loid) resistome variation than antibiotic resistome. The microbial community increased energy production-related metabolism to fulfill the increasing energy needs required by acid and heavy metal(loid) resistance. Horizontal gene transfer (HGT) events primarily exchanged energy- and information-related genes to adapt to the harsh AMD environment. These findings provide new insight into the risk of ARG proliferation in mining environments.

* Corresponding author at: State Key Laboratory of Environmental Geochemistry, Institute of Geochemistry, Chinese Academy of Sciences, Guiyang 550081, PR China.
E-mail address: haolikai@mail.gyig.ac.cn (L. Hao).
[1] L. Hao and C. Jiang shared co-corresponding authorship.

http://dx.doi.org/10.1016/j.scitotenv.2023.162330
Received 28 November 2022; Received in revised form 7 February 2023; Accepted 15 February 2023
Available online 20 February 2023

1. Introduction

The environmental proliferation of antibiotic resistance genes (ARG) has received increasing attention for its involvement in antibiotic resistance and treatment failure. This issue poses a threat to the health of humans and other organisms and is associated with huge economic losses and high mortality (Hendriksen et al., 2019; Zhuang et al., 2021). The number of annual deaths caused by antibiotic-resistant infections is estimated at least 700,000 and is predicted to increase to 10 million by 2050 if effective control measures are not implemented (Crofts et al., 2017). Current research indicates that other nonantibiotic agents, such as heavy metal(loid)s, can also promote ARG co-occurrence, which is called the co-selection of antibiotics and heavy metal(loid)s (Imran et al., 2019). The theory of co-selection states that heavy metal(loid) contamination can induce the co-occurrence of MRGs and ARGs through co-resistance, cross-resistance, and co-regulation (Li et al., 2017; Pal et al., 2017; Wales and Davies, 2015), thus it was hypothesized that mining environments are hotspots for both MRGs and ARGs.

Several regional studies have been conducted. A copper mine tailing-polluted soil was dominated by rifamycin-, glycopeptide aminocoumarin-, and macrolide-related resistance (Jiang et al., 2021), while MLS- (macrolides-lincosamides-streptogramins-), vancomycin-, and aminoglycoside-related resistance dominated the antibiotic resistome of a gold tailing-polluted farmland (Qiao et al., 2021). Besides, this hypothesis was confirmed thoroughly by a recent global-scale study on resistomes in mining environments, which identified a multidrug-dominated antibiotic resistome with an abundance similar to urban sewage but much higher than freshwater sediment (Yi et al., 2022). Given that mining sites could serve as potential hotspots for MRGs and ARGs, these results have raised concern about the risk of ARG environmental proliferation in these regions. While Yi et al. (2022) provided some new insight into mining environment resistomes, this study did not investigate the presence of resistomes in surrounding environments that are not directly impacted by mining activities. Thus, mining activities' influence on resistome dynamics remains unclear, which limits the understanding of the risk of ARG environmental proliferation.

Coal comprises >50 % of China's primary energy resources (Ma et al., 2020) and is predicted to contribute to >24 % of primary global energy by 2035 (Liu and Liu, 2020). The long-term high-intensity coal mining and the increasing demand will likely generate more associated pollutants, such as acid mine drainage (AMD). Under mediation by acidophilic microorganisms, when sulfide minerals (e.g., pyrite) in tailings combine with air and water, drainage with extremely low pH (<4), a high SO_4^{2-} concentration, and metal(loid) ions, appear (Dopson and Holmes, 2014; Pan et al., 2021; Xin et al., 2021). Since metal(loid)s are more soluble at acidic pH (Dopson and Holmes, 2014), microorganisms are required to resist higher heavy metal(loid) pressure in AMD than in regular aquatic environments. According to the co-selection theory, this will result in the co-occurrence of ARGs and MRGs. Thus, it is likely that coal-source AMD and AMD-affected soil include a high number of both ARGs and MRGs. Our recent study also found that coal source AMD holds abundant and high diverse resistomes (Huang et al., 2023).

To understand how mining activities influence the resistomes dynamics, a case study was conducted in a coal mine in Guizhou province, southern China. The resistomes in soil samples affected by flowing AMD and those from surrounding unaffected areas were assessed. Metagenomic techniques were used in three ways: (1) to investigate and compare the profiles of the antibiotic resistome, heavy metal(loid) resistome and mobile genetic elements (MGEs) in the two sample types, (2) to analyze the contribution of the microbial community and MGEs to the dynamics of the two resistomes, and (3) to measure energy production metabolism and assess potential HGT at the metagenome-assembled genome (MAG) level. The findings will improve our knowledge of resistome dynamics and survival strategies of the microbial community under acidic, multimetal(loid) enriched AMD contaminated conditions and inform an evaluation of the ARG dissemination risks of coal-source AMD.

2. Materials and methods

2.1. Sampling collection and processing

The coal mine of this study was located in Guizhou Province, Southwestern China (Fig. 1). AMD flows from the mine to the foot of a hill. Six AMD-affected soil samples were collected from the slope where AMD flowed, and five AMD-unaffected soil samples were collected from the surrounding woodlands 500–2000 m away from the AMD-flowing slope. About 50 g of soil was collected from each sampling site using the iron shovel and moved into a 50 ml aseptic centrifuge tube. The iron shovel was cleaned with 97 % alcohol and dried before sampling. All eleven samples were stored at 4 °C and sent to a lab within 1 h for subsequent experiments. Each sample was divided into two parts, one for pH determination and the other for DNA extraction and metagenomic sequencing. For pH determination, soil samples were air dried for at least 2 days, mixed with pure water (1:3, w/v), and the pH was determined using a pH meter. Other samples were placed in a foam box mixed with dry ice and sent to Guangdong Magigene Biotechnology Co. Ltd. for DNA extraction and metagenomic sequencing. Total DNA was extracted with a MagaBio soil/feces genomic DNA purification kit according to the manufacturer's instructions. The DNA was then used to construct a sequencing library on the HiSeq2500 platform (Illumina) using a 150 bp paired-end model with a minimum sequencing depth of ~10 Gb, which is deep enough for AMD-like extreme environments to conduct metagenomic assembly.

2.2. Raw sequence analysis

Raw sequences from each sample were independently processed. The kneaddata pipeline (v0.6.1) (github.com/biobakery/kneaddata) embedded with trimmomatic (v0.39) (Bolger et al., 2014) was used for quality control (key parameters were set as –trimmomatic-options' ILLUMINACLIP: adapters/TruSeq3-PE.fa:2:40:15 SLIDINGWINDOW:4:20 MINLEN:50′). For microbial community annotation, small subunit ribosomal RNAs (SSU rRNAs) of metagenomic sequences were reconstructed and annotated using phyloFlash with the identity set at 0.6 (Gruber-Vodicka et al., 2020). The OTUs annotated to bacteria or archaea were used for further analysis, while the fungi-like OTUs were filtered out. Quality reads were assembled into contigs with MEGAHIT (v1.1.3, kmer was set as –k-min 27 –k-max 141 –k-step 12, minimum length of 200 bp) (Li et al., 2015). Contigs longer than 200 bp were then used to determine ORF prediction, redundancy, and quantity using prodigal with default parameters (v2.6.3) (Hyatt et al., 2010), CD-HIT (v4.8.1, -aS 0.9 -c 0.95 -G 0 -g 0 -T 0 -M 0) (Fu et al., 2012) and salmon with default parameters (v0.13.1) (Patro et al., 2017), respectively. The abundance (coverage, ×/Gb) of RGs or MGEs in each sample was calculated using the following Formula (a) (Zhao et al., 2020a):

$$Abundance\ (coverage, \times/Gb) = \Sigma_1^n \frac{N_{mapped\ reads} \times L_{reads} / L_{RG/MGE\ -\ like\ ORF}}{S} \quad (a)$$

where $N_{mapped\ reads}$ is the number of the reads mapped to RG/MGE-like ORFs, L_{reads} is the sequence length of the Illumina reads (150 in the current study), $L_{RG/MGE\text{-}like\ ORF}$ is the sequence length of target RG/MGE-like ORFs, n is the number of the RG/MGE-like ORFs belonging to the same RG/MGE types, which was calculated by salmon in this study, and S is the size of the data set (Gb), which is the average of clean forward and clean reverse reads from every sample.

RGs/MGEs-like ORFs were recovered by blasting ORFs to the SARG database (Yin et al., 2018), BacMet2 database (Pal et al., 2014) and MobileGeneitcElementDatabase (Pärnänen et al., 2018) using diamond (blastp model for ARG and MRG blasting) or blast (blastn model for MGE blasting) (identity ≥ 70 %, e value = 10^{-5}, alignment length ≥ 18). The CARD database was used as the reference for classifying ARG mechanisms (Jia et al., 2017).

Fig. 1. Sampling sites. Six AMD affected soil samples (blue dots) were collected from slope where AMD flowed, while five AMD unaffected background soil samples (orange dots) were collected from surrounding woodlands 500–2000 m far away from the slope.

Five AMD-affected samples with contigs >1000 bp were chosen for MAG assembly using the MetaWRAP pipeline (v1.3.2) (Uritskiy et al., 2018). The pipeline includes several modules and can conduct MAG assembly, refinement, and quantitation separately. CheckM software (v1.0.12) was used to determine MAG completeness and contamination. DRep was then used to dereplicate MAGs, with relative parameters of -sa 0.99 -nc 0.30 -p 24 -comp 50 -con 5 (Olm et al., 2017). Middle- and high-quality dereplicated MAGs (contamination <5 %, completeness >50 %) were used to detect RGs/MGEs and MAG taxonomy annotation was conducted using gtdbtk (v1.6.0) with a reference database (version release_207) (Parks et al., 2022). Metachip with default parameters was used to detect potential HGT events between the dereplicated MAGs (Song et al., 2019).

DiTing was used to compare the biogeochemical pathways between groups (Xue et al., 2021). The relative abundance of a gene and a pathway was calculated using the following Formulas (b) and (c):

$$TPM_i = \frac{b_i}{\Sigma_j b_j} \cdot 10^6 = \frac{\frac{X_i}{L_i}}{\Sigma_j \frac{X_j}{L_j}} \cdot 10^6 \quad \text{(b)}$$

$$A_i = \frac{a_{1\_1} + a_{1\_2} + a_{1\_n}}{n} + \frac{a_{2\_1} + a_{2\_2} + \ldots + a_{2\_n}}{n} + \ldots + \frac{a_{m\_1} + a_{m\_2} + \ldots + a_{m\_n}}{n} \quad \text{(c)}$$

where for Formula (b), TPM_i indicates the relative abundance of gene i, b_i represents the copy number of gene i, Li represents the length of gene I, X_i indicates the number of times that gene i is detected in a sample, and j is the number of genes in a sample. For Formula (c), Ai indicates the relative abundance of the i pathway, a_{m_n} is the relative abundance of protein m_n in each sample, m is one of the optional routes for accomplishing the i pathway, and n is the number of proteins in the optional route, m.

2.3. Statistical analysis and visualization

R (v3.6.1) and Excel (version 2019) were used to conduct statistical analysis and visualization. All pictures were adjusted using Adobe Illustrator (version CC 2019).

Barplots were drawn on the free online ImageGP platform (Chen et al., 2022a). Procrustes and correlation heatmap analyses were performed using the *Spearman* method on the free online Tutools platform (cloudtutu.com). The online platform, iTOL (itol.embl.de), was used to draw a MAG phylogenetic tree and the annotation files were produced using R. Heatmaps were drawn using the R "pheatmap" package (v1.0.12). An HGT network was drawn using Gephi software (v0.9). The student *t*-test was used to measure the ANOVA between contaminated and background soils. "*", "**" and "***" represented p-values of "≤0.1", "≤0.05" and "≤0.01", respectively.

3. Results

3.1. ARG variation

The pH values were between 3.34–5.03 in the background and 2.9–3.1 in contaminated soils, which is understandable given that extremely acidic AMD can intensely lower soil pH.

Strong variation in the antibiotic resistome between the background and contaminated soils was shown in Fig. 2, Fig. S1a and Table S1. The average abundance decreased from 85.47 ± 19.71 ×/Gb in background soils to 47.45 ± 23.34 ×/Gb in contaminated soils (p = 0.0266**). More types of antibiotic resistance were detected in the background than in contaminated soils (16 and 14, respectively), as sulfonamide and carbomycin resistance was not detected later. 82 kinds of ARGs were detected in background soils, while only 45 were found in contaminated soils. Multidrug resistance was dominant, with an average percentage in the background and contaminated soils of 68.85 % ± 6.10 % and 84.13 % ± 3.30 %, respectively (p = 0.004***). Multidrug resistance also included most kinds of ARGs (29 and 21 for background and contaminated soils, respectively). In the two types of soils, *mdtB* and *mdtC* were the top two most abundant ARGs, occupying 43.70 % and 56.16 % of background and contaminated soils, respectively.

3.2. MRG and MGE variation

Differences in the heavy metal(loid) resistome between background and contaminated soils are shown in Fig. 3a, Fig. S1b, and Table S2. The average abundance increased from 85.30 ± 4.36 ×/Gb in background soils to 133.29 ± 29.36 ×/Gb in contaminated soils (p = 0.014082**), by 56.26 %. 17 heavy metal(loid) types were detected in background soils and 15 in contaminated soils, as Cd and Te resistance were not detected later. In addition, 102 MRG types were detected in background soils, while 79 were in contaminated soils. The four most abundant heavy metal(loid) resistance types were Hg-resistance, multimetal(loid)s-resistance, Cu-resistance and Fe-resistance. Their average abundance increased from 0.49 ×/Gb, 13.56 ×/Gb, 10.43 ×/Gb and 19.856 ×/Gb in background soils to 34.68 ×/Gb, 29.50 ×/Gb, 19.06 ×/Gb and 24.328 ×/Gb in contaminated soils, respectively. Among the MRGs, Hg resistance-related *merA* increased most significantly from 0.20 ×/Gb in background soils to 21.95 ×/Gb in contaminated soils, followed by multimetal(loid)s-resistance-related *ruvB* (resist Cr-Se-Te), which increased from 2.20 ×/Gb

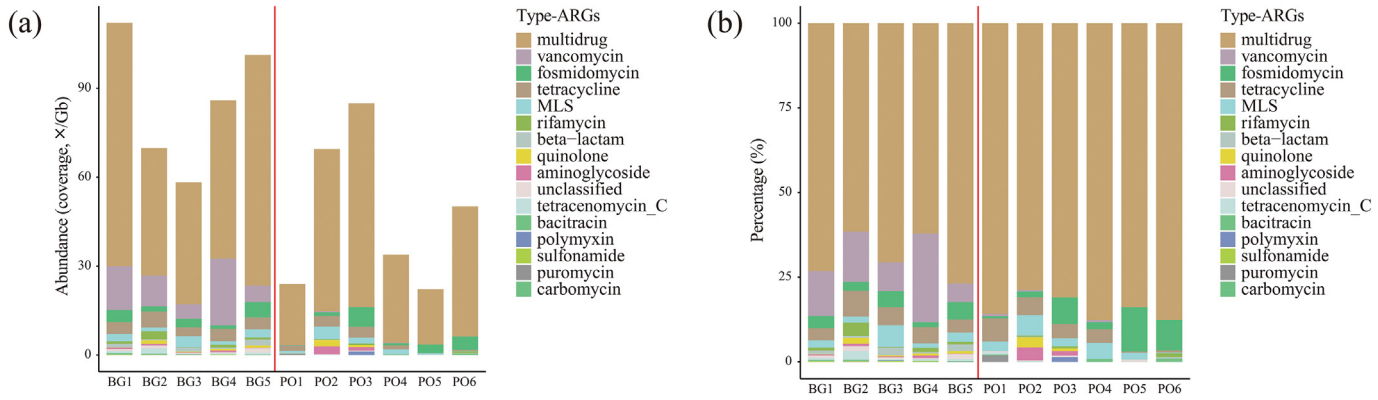

Fig. 2. Differences in the (a) relative abundance and (b) percentage of the antibiotic resistome between background and AMD contamination areas, by ARG type; BG represents background samples, and PO represents AMD contaminated samples.

to 14.75 ×/Gb, Fe-resistance-related *dpsA*, which increased from 0.056 ×/Gb to 12.20 ×/Gb, and Hg-resistance-related *merT*, which increased from 0.244 ×/Gb to 8.570 ×/Gb.

Differences in MGE levels between background and contaminated soils are shown in Fig. 3b, Fig. S1c and Table S3. The average abundance increased from 36.81 ± 6.25 ×/Gb in background soils to 188.51 ± 21.81 ×/Gb in contaminated soils (p = 5.95E−06***), by 412.12 %. Four MGE types, transposase, insertion_sequences, transposition_module, and integrase, were detected in background soils, while a new type of plasmid was detected in contaminated soils. In addition, 21 MGE types were detected in background soils and 23 in contaminated soils. Two abundant MGE types were transposase and insertion_sequences, whose average abundance increased from 19.91 ×/Gb and 15.71 ×/Gb in background soils to 108.53 ×/Gb and 77.46 ×/Gb in contaminated soils, respectively. *TnpA*, *IS91* and *ISRj1* contributed to the highest levels of MGE accumulation, increasing from 18.91 ×/Gb, 10.79 ×/Gb and 1.21 ×/Gb in background soils to 89.89 ×/Gb, 47.51 ×/Gb, and 18.19 ×/Gb in contaminated soils, respectively.

3.3. The driving effects of the microbial community and MGEs on ARGs and MRGs

Genera, MGEs, ARGs, and MRGs were horizontally clustered into two groups based on sampling area (Fig. 4), indicating that AMD contamination significantly changed their organization (genus annotation is shown in Table S4).

The sum of square (M^2) was much lower between Genera and MRGs (0.3753; p = 0.001***) than between Genera and ARGs (0.8289; p = 0.045**). Similarly, MGEs and MRGs had a smaller M^2 (0.2088; p = 0.001***) than MGEs and ARGs (0.6956; p = 0.021**). Significant smaller M^2 of the Genera and MGEs to MRGs than ARGs indicated that the microbial community at the genera level and MGEs exhibited a more significant influence on MRGs dynamics than ARGs.

3.4. Variations in energy production-related metabolism

Differences in energy production-related metabolic pathways are shown in Fig. 5 and Fig. S2. The average abundances of most energy-related metabolic pathways were higher in AMD-contaminated soils than in background soils. For carbon (Table S5), the Enter-Doudoroff (ED) pathway increased from 63.79 ± 19.998 TPM to 108.912 ± 12.662 TPM (corrected p = 0.0227; all of the p values in late were corrected), TCA increased from 53.063 ± 17.492 TPM to 191.273 ± 25.21 TPM (p = 1e−04), and glycolysis increased from 91.728 ± 10.461 TPM to 230.88 ± 15.998 TPM in contaminated and background soils, respectively (p = 0***). Several fermentation pathways also increased. For nitrogen (Table S6), three denitrification pathways, including nitrate to nitrite, nitrite to nitric oxide and nitric oxide to nitrous oxide, increased from 9.768 ± 9.256 TPM, 12.021 ± 11.588 TPM and 17.402 ± 13.665 TPM in contaminated soil to 12.724 ± 6.399 TPM, 33.593 ± 6.563 TPM, 34.229 ± 8.877 TPM in background soil, respectively, although the difference was not significant (p > 0.05). For sulfur (Table S7), two dissimilatory sulfate reduction pathways, including sulfate to sulfite conversion and sulfite to sulfide conversion, increased from 43.277 ± 16.343 TPM and 2.152 ± 2.673 TPM to 153.75 ± 25.573 TPM (p = 3e−04***) and 8.2 ± 2.792 TPM (p = 0.0212**) in contaminated and background soils, respectively.

3.5. Horizontal gene transfer (HGT) events

107 middle and highly complete dereplicated MAGs were recovered (Fig. S3 and Table S9), including 59 bacterial and 48 archaeal MAGs. 130 HGT events were detected between or within 13 phyla (Fig. 6a and

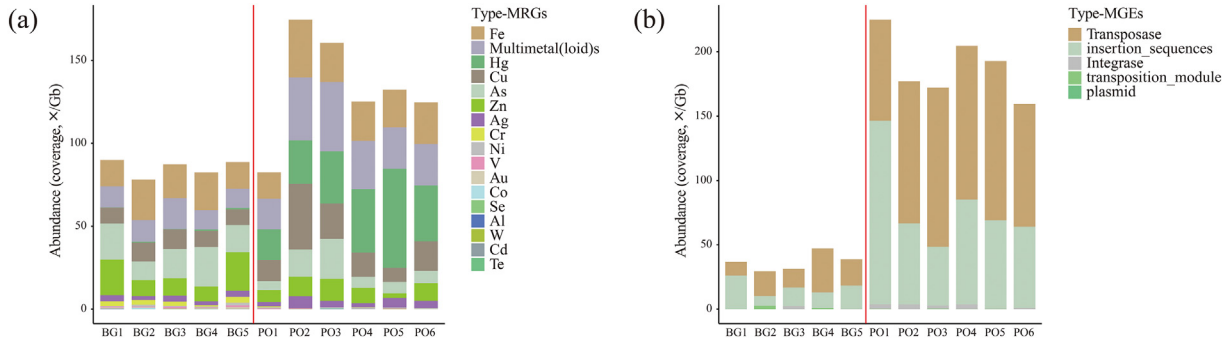

Fig. 3. Variations in (a) heavy metal(loid)s and (b) MGEs between the background and AMD contamination areas by type; BG represents background samples, and PO represents AMD contaminated samples.

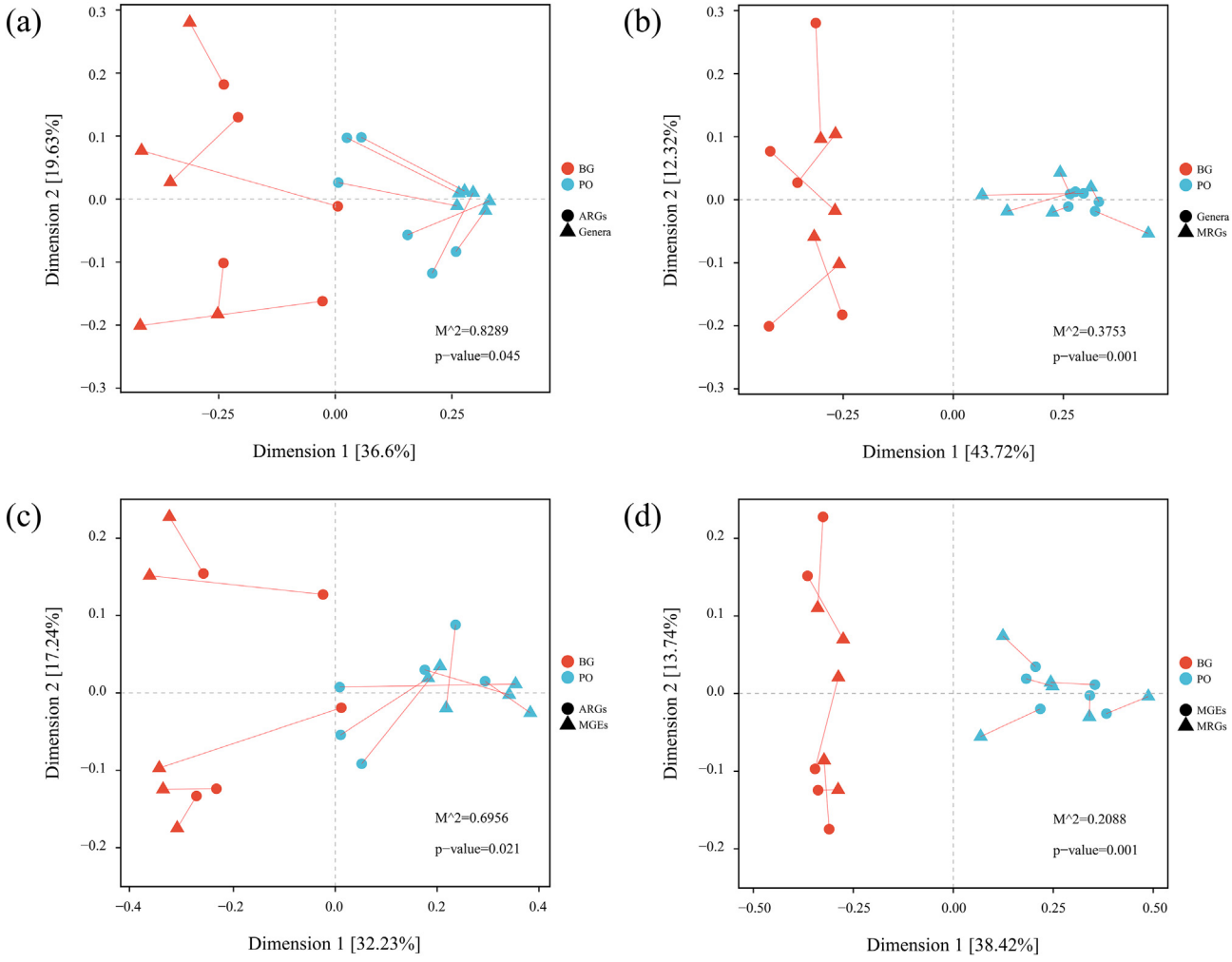

Fig. 4. Procrustes analysis comparing (a) Genera and ARGs, (b) Genera and MRGs, (c) MGEs and ARGs, and (d) MGEs and MRGs; BG represents background samples, and PO represents AMD contaminated samples. A smaller M^2 represents higher similarity, and the P-value represents M^2 significance. Genera annotation and abundance are found in Table S4.

Table S11). Notably, HGT events occurred more frequently within the same kingdom, which was higher for archaea-archaea (n = 10) and bacteria-bacteria (n = 115) than between archaea and bacteria (n = 5). 72 HGT events occurred within the same phylum, including 43 within proteobacteria, 16 within Acidobacteriota, eight within Actinobacteriota, three within Thermoproteota and two within Thermoplasmatota.

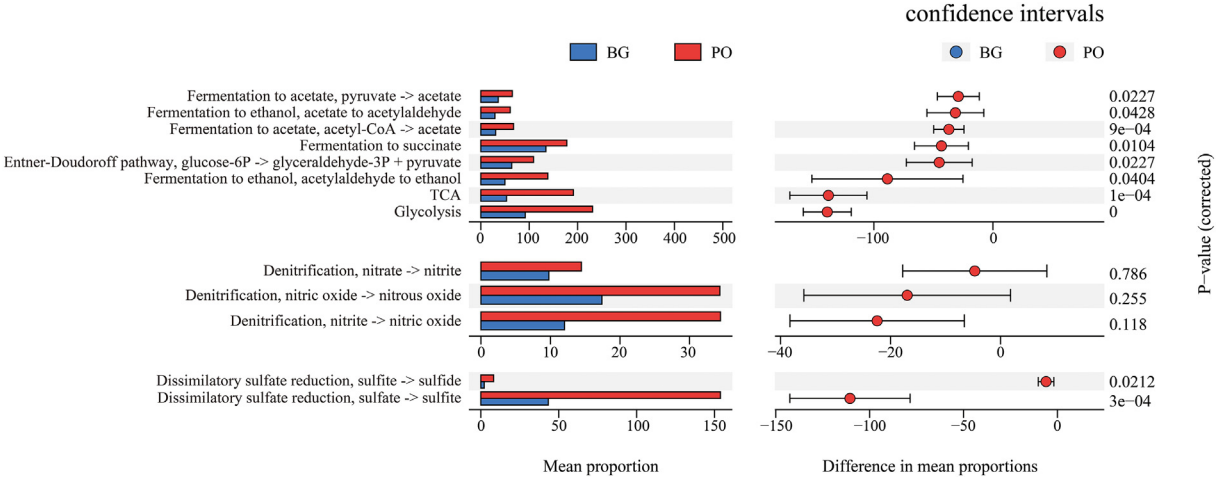

Fig. 5. Energy production-related metabolism. The unit of relative abundance was TMP and the P-value was adjusted using the BH method; the blue and red bars represent the average abundance of background and AMD contaminated samples. BG represents background samples, and PO represents AMD contaminated samples.

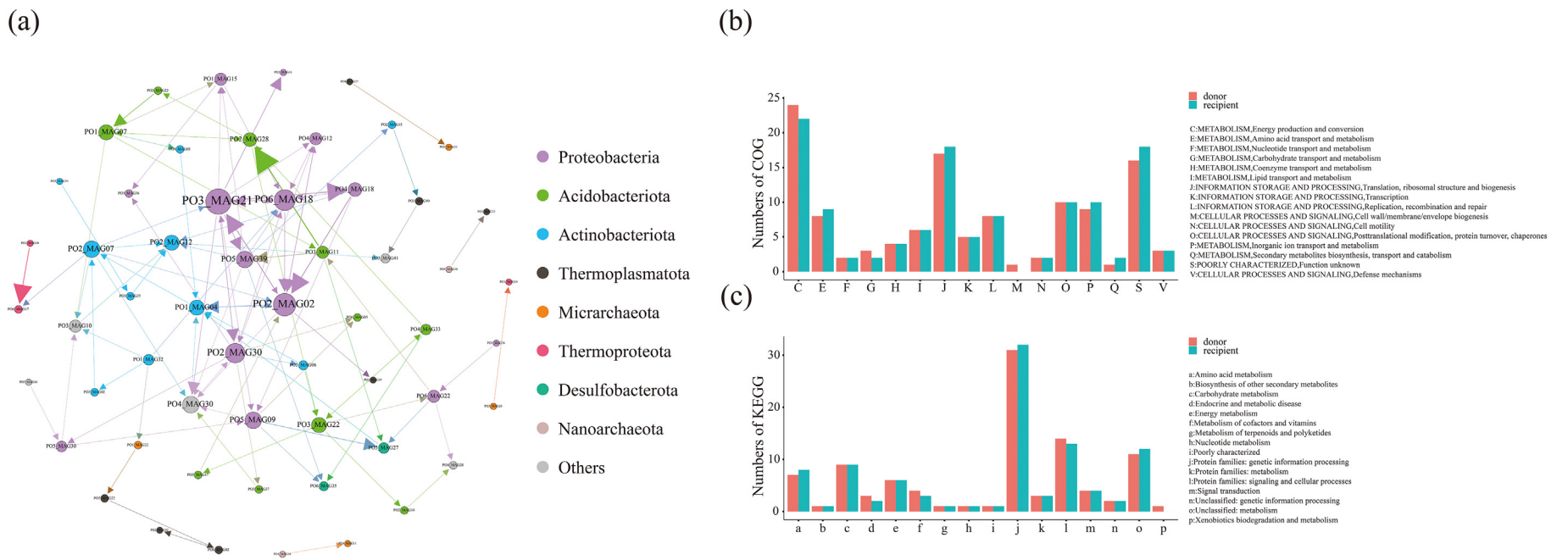

Fig. 6. HGT events and gene annotation. (a) The network representing HGT events included 107 MAGs; the arrow represents the transfer direction between the donor and recipient, the size of the arrow represents the number of genes transferred between the two MAGs, and the color represents the different MAG phyla. The annotation of genes involved in HGT events in the (b) COG and (c) KEGG databases; the red bar represents donor genes and the green bar represents recipient genes.

No HGT events were annotated as RGs or MGEs. COG annotation of 130 HGT events is shown in Fig. 6b and Table S12. There were no big differences between donor and recipient annotation. Most were annotated as c (energy production and conversion), with a frequency of 24 in donor and 22 in recipient, respectively, followed by J (translation, ribosomal structure, and biogenesis), with a frequency of 17 in donor and 18 in recipient.

KEGG annotation of 130 HGT events is shown in Fig. 6c and Table S13. The highest frequency occurred in j (genetic information processing), with a frequency of 31 in donor and 32 in recipient, followed by l (signaling and cellular processes), with a frequency of 14 in donor and 13 in recipient.

4. Discussion

4.1. Differences in the antibiotic resistome in AMD contaminated soils

ARGs associated with ore mining waste and iron bursts in Brazil were found to increase in amount and abundance following tailing dam disasters (Furlan et al., 2020), and accidental antimony contamination was associated with higher ARG levels (Chen et al., 2022b). Thus, it was hypothesized that multimetal(loid)-enriched AMD contamination would stimulate a similar increase in ARGs.

Unexpectedly, results from the current study showed that AMD contamination was associated with lower ARG diversity and abundance. In the studies discussed above, the pH values of samples were 6.4–7.1 (Furlan et al., 2020) and 8.5–9.5 (Chen et al., 2022b), respectively, which were considerably higher than the present study. In addition, the decrease in relative abundance and the ARGs types found in this study were similar to a study by Lin et al. (2020), which reported that acidic conditions enhance the removal of sulfonamide antibiotics and antibiotic resistance determinants from swine manure. These results imply that acidification likely leads to a decrease in antibiotic resistance.

The current study found that multidrug-resistance genes, including *mdtB* and *mdtC,* had the highest relative abundance. Most other studies also found that multidrug resistance genes occupied the highest relative abundance. Zhao et al. (2020b) and Malik et al. (2017) described the presence of a multidrug resistance-dominated antibiotic resistome in acidic soil environments, potentially due to the need for microbes in these settings to perform multiple functions such as maintaining pH homeostasis and resisting heavy metal(loid)s (Teelucksingh et al., 2020; Zgurskaya et al., 2021). While the current study showed a decrease in total ARG abundance, the proportion of multidrug resistance genes increased from 68.851 % ± 6.099 % in background soils to 84.129 % ± 3.302 % in contaminated soils. Thus, under acidic AMD environments, microbial communities appear to sequester a higher number of multifunctional multidrug-dominated ARGs as a survival strategy.

4.2. Differences in MRGs and MGEs under AMD contamination

An increase in MRG expression may be attributed to a rise in Hg-resistance-related *merA*, multimetal(loid)-resistance-related *ruvB*, Fe-resistance-related *dpsA* and Hg-resistance-related *merT*. *MerA* encodes mercuric reductase (SM et al., 2006) and participates in reducing Au^{3+} and Au^{+} (Summers and Sugarman, 1974). *MerT* encodes an inner membrane protein required for Hg(II) binding and full Hg(II) resistance (Hamlett et al., 1992), which also involves cadmium transport activity (Ohshiro et al., 2020). Pyrite, the primary metal sulfide in coal mines, is also the main host mineral of toxic Hg, which releases Hg into AMD environments through oxidative dissolution (Manceau et al., 2018), stimulating *merA* and *merT* enrichment to help microbial communities to resist Hg stress. *RuvB* is a multimetal resistance gene capable of resisting toxic, redox-active elements such as Cr, Se, and Te. Fe-related *dpsA* encodes a protein that can protect chromosomal DNA from oxidative damage, whose expression increases under the deficiency in particular nutrients, such as nitrogen or phosphorus (Michel et al., 2003). The enrichment of *dpsA* can help microorganisms survive in oligotrophic sites such as AMD (Chen et al., 2016). To sum up, microbial communities produce higher levels of multifunctional MRGs to resist the multimetal(loid)-enriched AMD environment.

4.3. Key factors driving resistome variability

This study found that MRGs increased with the decrease in ARGs, which is supported by other studies. For example, Xu et al. (2022) found that biophysical drying reduced ARGs abundance while increasing MRG expression and attributed this to the selection of MRG-carrying microorganisms.

Procrustes analysis (Fig. 4) showed that the microbial community and MGEs had a stronger correlation with MRGs than ARGs. The higher similarity found between the microbial community and MRGs (0.3753***) than ARGs (0.8289**) supports the opinions of Xu et al. (2022) that heavy metal(loid) pressures specifically selected for MRG-carrying microorganisms over ARG-carrying microorganisms. Meanwhile, the higher similarity between MGEs and MRGs (0.2088***) than between MGEs and ARGs (0.6956**) implies that MGEs mediated more MRG-related HGT events than ARG-related events in this scenario.

These findings suggest that microorganisms can transfer MRGs vertically from parent to offspring and horizontally through MGE-mediated HGT events to resist the pressure of toxic metal(loid)s.

4.4. Differences in energy metabolism

KEGG annotation showed that the microbial community produced higher levels of energy production-related metabolic products under AMD contamination. Organic carbon sources may originate from dead microorganisms unable to adapt to a changing environment. Meanwhile, intensified nitrate and sulfate reduction stimulate energy production. Similarly, antibiotic-mediated metabolic stimulation has been observed by Lopatkin et al. (2021), which was consistent with the theory of fitness costs.

Under the fitness costs theory, antibiotic resistance either disrupts important cellular processes or imposes large energetic burdens, as many antibiotics target these processes (Melnyk et al., 2015). Meanwhile, resistance mechanisms such as forming *mdtB*-, *mdtC*-efflux-dominated antibiotic resistome and metal(loid) resistance can consume part of a microbe's energy budget (Guazzaroni et al., 2013; Herren and Baym, 2022; Nanda et al., 2019). Thus, in the oligotrophy metal(loid) enriched AMD sites, RG-carrying microorganisms stimulated energy production-related metabolism to adapt to severe environments (Chen et al., 2015b).

4.5. HGT events at the MAG level

No RG-related HGT events were detected in 107 middle- and high-completeness dereplicated MAGs, which may be attributed to the limited numbers of recovered MAGs. Most COG annotations were energy production-and-conversion-, translation-, or ribosomal structure-and-biogenesis-related, while most KEGG annotations were genetic-information-processing- and signaling-and-cellular-processing-related. The annotation results suggest that in addition to RGs, microorganisms must acquire or reinforce other functions, such as acid tolerance, material transport, and metabolism by HGT, to adapt to harsh AMD environments (Chen et al., 2021; Guo et al., 2015).

Several studies have observed that metabolic genes (especially involved in mitigating the energetic demands of stress response) are shared among microorganisms through HGT mediated by conjugative plasmids when facing antibiotic pressure (Chen et al., 2015a; Schlüter et al., 2003). This study found a similar phenomenon that energy- and information-related genes frequently participated in HGT events mediated by MGEs.

A recently published study also reported that metabolic genes on conjugative plasmid are highly prevalent in clinically important *Escherichia coli* pathogens when facing antibiotic treatment (Palomino et al., 2023). These results might imply the undiscovered function of cellular metabolic processes on antibiotic or metal(loid) resistance and provide selective advantages.

4.6. Risk of MRG environmental proliferation

MRG expression is an environmental adaptation strategy that helps microorganisms resist multimetal(loid) pressure (Chandrangsu et al., 2017). However, some heavy metal(loid)s such as arsenic, cadmium, copper, mercury, silver, tellurium, and zinc are shown to have a similar function as traditional antibiotic therapies and have been used in clinics (Cheeseman et al., 2020). This has led to the emergence of heavy metal(loid) resistant pathogens and has fostered concerns about potential MRG environmental proliferation (Zagui et al., 2021).

This study observed a significant increase in MRGs in AMD contaminated areas. Thus, the risk of potential MRG environmental proliferation in these regions should be seriously considered.

5. Conclusion

A global study recently outlined the significant role of the multidrug resistance-dominated ARG resistome in mining-impacted environments. However, the impact of AMD contamination on resistomes has remained unknown, hindering an evaluation of the risk of ARG proliferation. The current study found that AMD contamination decreased the abundance of multidrug-dominated ARGs but increased MRG and MGE levels. Microbial communities and MGEs drove MRG variation but contributed little to ARGs. The microbial community reinforced energy metabolism to adapt to the AMD-contaminated environments. Broader comparative investigations of different mine environments are needed. In addition, proper attention should be paid to the risk of MRG proliferation in mine environments given the appearance of metal(loid)-resistance pathogens.

Supplementary data to this article can be found online at https://doi.org/10.1016/j.scitotenv.2023.162330.

CRediT authorship contribution statement

Qiang Huang: Writing – original draft, Methodology. **Zhenghua Liu:** Visualization, Software. **Yuan Guo:** Validation, Investigation. **Bao Li:** Validation, Investigation. **Zhenni Yang:** Data curation, Resources. **Xiaoling Liu:** Validation, Investigation. **Jianmei Ni:** Validation, Investigation. **Xiutong Li:** Validation, Investigation. **Xi Zhang:** Data curation, Resources. **Nan Zhou:** Data curation, Resources. **Huaqun Yin:** Experiment design. **Chengying Jiang:** Supervision, Funding acquisition, Conceptualization. **Likai Hao:** Supervision, Funding acquisition, Conceptualization.

Data availability

Data will be made available on request.

Declaration of competing interest

The authors declare that they have no known competing financial interests or personal relationships that could have appeared to influence the work reported in this paper.

Acknowledgements

This work was supported by grants from the Guizhou Provincial Department of Science and Technology (E2DF028), the National Key Research and Development Project of China (2018YFC1802601), the National Natural Science Foundation of China (91851206, 41877400), Startup Funding of the Chinese Academy of Sciences (2017-020), the Joint Funds of Innovation Academy for Green Manufacture, Chinese Academy of Sciences (IAGM2020C24), the CAS Engineering Laboratory for Advanced Microbial Technology of Agriculture, Chinese Academy of Sciences (KFJ-PTXM-016), CAS–NSTDA Joint Research Project (153211KYSB20200039), the State Key Laboratory of Environmental Geochemistry (SKLEG2018911), and the State Key Laboratory of Microbial Technology Foundation (M2017-01).

References

Bolger, A.M., Lohse, M., Usadel, B., 2014. Trimmomatic: a flexible trimmer for Illumina sequence data. Bioinformatics 30, 2114–2120.
Chandrangsu, P., Rensing, C., Helmann, J.D., 2017. Metal homeostasis and resistance in bacteria. Nat. Rev. Microbiol. 15, 338–350.
Cheeseman, S., Christofferson, A.J., Kariuki, R., Cozzolino, D., Daeneke, T., Crawford, R.J., Truong, V.K., Chapman, J., Elbourne, A., 2020. Antimicrobial metal nanomaterials: from passive to stimuli-activated applications. Adv.Sci. 7, 1902913.
Chen, K., Xu, X., Zhang, L., Gou, Z., Li, S., Freilich, S., Jiang, J., 2015a. Comparison of four comamonas catabolic plasmids reveals the evolution of pBHB to catabolize haloaromatics. Appl. Environ. Microbiol. 82, 1401–1411.
Chen, L.X., Hu, M., Huang, L.N., Hua, Z.S., Kuang, J.L., Li, S.J., Shu, W.S., 2015b. Comparative metagenomic and metatranscriptomic analyses of microbial communities in acid mine drainage. ISME J. 9, 1579–1592.
Chen, L.X., Huang, L.N., Méndez-García, C., Kuang, J.L., Hua, Z.S., Liu, J., Shu, W.S., 2016. Microbial communities, processes and functions in acid mine drainage ecosystems. Curr. Opin. Biotechnol. 38, 150–158.
Chen, Z., Liu, W.S., Zhong, X., Zheng, M., Fei, Y.H., He, H., Ding, K., Chao, Y., Tang, Y.T., Wang, S., Qiu, R., 2021. Genome- and community-level interaction insights into the ecological role of archaea in rare earth element mine drainage in South China. Water Res. 201, 117331.
Chen, T., Liu, Y.-X., Huang, L., 2022a. ImageGP: an easy-to-use data visualization web server for scientific researchers. iMeta 1, e5.
Chen, X., Wang, J., Pan, C., Feng, L., Guo, Q., Chen, S., Xie, S., 2022b. Metagenomic analysis reveals the response of microbial community in river sediment to accidental antimony contamination. Sci. Total Environ. 813, 152484.
Crofts, T.S., Gasparrini, A.J., Dantas, G., 2017. Next-generation approaches to understand and combat the antibiotic resistome. Nat. Rev. Microbiol. 15, 422–434.
Dopson, M., Holmes, D.S., 2014. Metal resistance in acidophilic microorganisms and its significance for biotechnologies. Appl. Microbiol. Biotechnol. 98, 8133–8144.
Fu, L., Niu, B., Zhu, Z., Wu, S., Li, W., 2012. CD-HIT: accelerated for clustering the next-generation sequencing data. Bioinformatics 28, 3150–3152.
Furlan, J.P.R., Dos Santos, L.D.R., Moretto, J.A.S., Ramos, M.S., Gallo, I.F.L., Alves, G.A.D., Paulelli, A.C., Rocha, C.C.S., Cesila, C.A., Gallimberti, M., Devóz, P.P., Júnior, F.B., Stehling, E.G., 2020. Occurrence and abundance of clinically relevant antimicrobial resistance genes in environmental samples after the Brumadinho dam disaster,Brazil. Sci. Total Environ. 726, 138100.
Gruber-Vodicka, H.R., Seah, B.K.B., Pruesse, E., 2020. phyloFlash: rapid small-subunit rrna profiling and targeted assembly from metagenomes. mSystems 5.
Guazzaroni, M.E., Morgante, V., Mirete, S., González-Pastor, J.E., 2013. Novel acid resistance genes from the metagenome of the Tinto River, an extremely acidic environment. Environ. Microbiol. 15, 1088–1102.
Guo, J., Wang, Q., Wang, X., Wang, F., Yao, J., Zhu, H., 2015. Horizontal gene transfer in an acid mine drainage microbial community. BMC Genomics 16, 496.
Hamlett, N.V., Landale, E.C., Davis, B.H., Summers, A.O., 1992. Roles of the Tn21 merT, merP, and merC gene products in mercury resistance and mercury binding. J. Bacteriol. 174, 6377–6385.
Hendriksen, R.S., Munk, P., Njage, P., van Bunnik, B., McNally, L., Lukjancenko, O., Röder, T., Nieuwenhuijse, D., Pedersen, S.K., Kjeldgaard, J., Kaas, R.S., Clausen, P., Vogt, J.K., Leekitcharoenphon, P., van de Schans, M.G.M., Zuidema, T., de Roda Husman, A.M., Rasmussen, S., Petersen, B., Amid, C., Cochrane, G., Sicheritz-Ponten, T., Schmitt, H., Alvarez, J.R.M., Aidara-Kane, A., Pamp, S.J., Lund, O., Hald, T., Woolhouse, M., Koopmans, M.P., Vigre, H., Petersen, T.N., Aarestrup, F.M., 2019. Global monitoring of antimicrobial resistance based on metagenomics analyses of urban sewage. Nat. Commun. 10, 1124.
Herren, C.M., Baym, M., 2022. Decreased thermal niche breadth as a trade-off of antibiotic resistance. ISME J. 16, 1843–1852.
Huang, Q., Huang, Y., Li, B., Li, X., Guo, Y., Jiang, Z., Liu, X., Yang, Z., Ning, Z., Xiao, T., Jiang, C., Hao, L., 2023. Metagenomic analysis characterizes resistomes of an acidic, multimetal (loid)-enriched coal source mine drainage treatment system. J. Hazard. Mater. 448, 130898.
Hyatt, D., Chen, G.L., Locascio, P.F., Land, M.L., Larimer, F.W., Hauser, L.J., 2010. Prodigal: Prokaryotic gene recognition and translation initiation site identification. BMC Bioinformatics 11, 119.
Imran, M., Das, K.R., Naik, M.M., 2019. Co-selection of multi-antibiotic resistance in bacterial pathogens in metal and microplastic contaminated environments: an emerging health threat. Chemosphere 215, 846–857.
Jia, B., Raphenya, A.R., Alcock, B., Waglechner, N., Guo, P., Tsang, K.K., Lago, B.A., Dave, B.M., Pereira, S., Sharma, A.N., Doshi, S., Courtot, M., Lo, R., Williams, L.E., Frye, J.G., Elsayegh, T., Sardar, D., Westman, E.L., Pawlowski, A.C., Johnson, T.A., Brinkman, F.S., Wright, G.D., McArthur, A.G., 2017. CARD 2017: expansion and model-centric curation of the comprehensive antibiotic resistance database. Nucleic Acids Res. 45, D566–d573.
Jiang, X., Liu, W., Xu, H., Cui, X., Li, J., Chen, J., Zheng, B., 2021. Characterizations of heavy metal contamination, microbial community, and resistance genes in a tailing of the largest copper mine in China. Environ. Pollut. 280, 116947.
Li, D., Liu, C.M., Luo, R., Sadakane, K., Lam, T.W., 2015. MEGAHIT: an ultra-fast single-node solution for large and complex metagenomics assembly via succinct de Bruijn graph. Bioinformatics 31, 1674–1676.
Li, L.G., Xia, Y., Zhang, T., 2017. Co-occurrence of antibiotic and metal resistance genes revealed in complete genome collection. ISME J. 11, 651–662.
Lin, H., Sun, W., Yu, Q., Ma, J., 2020. Acidic conditions enhance the removal of sulfonamide antibiotics and antibiotic resistance determinants in swine manure. Environ. Pollut. 263, 114439.
Liu, T., Liu, S., 2020. The impacts of coal dust on miners' health: a review. Environ. Res. 190, 109849.

Lopatkin, A.J., Bening, S.C., Manson, A.L., Stokes, J.M., Kohanski, M.A., Badran, A.H., Earl, A.M., Cheney, N.J., Yang, J.H., Collins, J.J., 2021. Clinically relevant mutations in core metabolic genes confer antibiotic resistance. Science 371.

Ma, Q., Nie, W., Yang, S., Xu, C., Peng, H., Liu, Z., Guo, C., Cai, X., 2020. Effect of spraying on coal dust diffusion in a coal mine based on a numerical simulation. Environ. Pollut. 264, 114717.

Malik, A.A., Thomson, B.C., Whiteley, A.S., Bailey, M., Griffiths, R.I., 2017. Bacterial physiological adaptations to contrasting edaphic conditions identified using landscape scale metagenomics. Mbio 8.

Manceau, A., Merkulova, M., Murdzek, M., Batanova, V., Baran, R., Glatzel, P., Saikia, B.K., Paktunc, D., Lefticariu, L., 2018. Chemical forms of mercury in pyrite: implications for predicting mercury releases in acid mine drainage settings. Environ.Sci.Technol. 52, 10286–10296.

Melnyk, A.H., Wong, A., Kassen, R., 2015. The fitness costs of antibiotic resistance mutations. Evol. Appl. 8, 273–283.

Michel, K.P., Berry, S., Hifney, A., Kruip, J., Pistorius, E.K., 2003. Adaptation to iron deficiency: a comparison between the cyanobacterium Synechococcus elongatus PCC 7942 wild-type and a DpsA-free mutant. Photosynth. Res. 75, 71–84.

Nanda, M., Kumar, V., Sharma, D.K., 2019. Multimetal tolerance mechanisms in bacteria: the resistance strategies acquired by bacteria that can be exploited to 'clean-up' heavy metal contaminants from water. Aquat. Toxicol. 212, 1–10.

Ohshiro, Y., Uraguchi, S., Nakamura, R., Takanezawa, Y., Kiyono, M., 2020. Cadmium transport activity of four mercury transporters (MerC, MerE, MerF and MerT) and effects of the periplasmic mercury-binding protein MerP on Mer-dependent cadmium uptake. FEMS Microbiol. Lett. 367.

Olm, M.R., Brown, C.T., Brooks, B., Banfield, J.F., 2017. dRep: a tool for fast and accurate genomic comparisons that enables improved genome recovery from metagenomes through de-replication. ISME J. 11, 2864–2868.

Pal, C., Bengtsson-Palme, J., Rensing, C., Kristiansson, E., Larsson, D.G., 2014. BacMet: antibacterial biocide and metal resistance genes database. Nucleic Acids Res. 42, D737–D743.

Pal, C., Asiani, K., Arya, S., Rensing, C., Stekel, D.J., Larsson, D.G.J., Hobman, J.L., 2017. Metal resistance and its association with antibiotic resistance. Adv. Microb. Physiol. 70, 261–313.

Palomino, A., Gewurz, D., DeVine, L., Zajmi, U., Moralez, J., Abu-Rumman, F., Smith, R.P., Lopatkin, A.J., 2023. Metabolic genes on conjugative plasmids are highly prevalent in Escherichia coli and can protect against antibiotic treatment. ISME J. 17, 151–162.

Pan, Y., Ye, H., Li, X., Yi, X., Wen, Z., Wang, H., Lu, G., Dang, Z., 2021. Spatial distribution characteristics of the microbial community and multi-phase distribution of toxic metals in the geochemical gradients caused by acid mine drainage, South China. Sci. Total Environ. 774, 145660.

Parks, D.H., Chuvochina, M., Rinke, C., Mussig, A.J., Chaumeil, P.A., Hugenholtz, P., 2022. GTDB: an ongoing census of bacterial and archaeal diversity through a phylogenetically consistent, rank normalized and complete genome-based taxonomy. Nucleic Acids Res. 50, D785–d794.

Pärnänen, K., Karkman, A., Hultman, J., Lyra, C., Bengtsson-Palme, J., Larsson, D.G.J., Rautava, S., Isolauri, E., Salminen, S., Kumar, H., Satokari, R., Virta, M., 2018. Maternal gut and breast milk microbiota affect infant gut antibiotic resistome and mobile genetic elements. Nat. Commun. 9, 3891.

Patro, R., Duggal, G., Love, M.I., Irizarry, R.A., Kingsford, C., 2017. Salmon provides fast and bias-aware quantification of transcript expression. Nat. Methods 14, 417–419.

Qiao, L., Liu, X., Zhang, S., Zhang, L., Li, X., Hu, X., Zhao, Q., Wang, Q., Yu, C., 2021. Distribution of the microbial community and antibiotic resistance genes in farmland surrounding gold tailings: a metagenomics approach. Sci. Total Environ. 779, 146502.

Schlüter, A., Heuer, H., Szczepanowski, R., Forney, L.J., Thomas, C.M., Pühler, A., Top, E.M., 2003. The 64 508 bp IncP-1beta antibiotic multiresistance plasmid pB10 isolated from a waste-water treatment plant provides evidence for recombination between members of different branches of the IncP-1beta group. Microbiology (Reading) 149, 3139–3153.

SM, N.C., Schaefer, J.K., Crane, S., Zylstra, G.J., Barkay, T., 2006. Analysis of mercuric reductase (merA) gene diversity in an anaerobic mercury-contaminated sediment enrichment. Environ. Microbiol. 8, 1746–1752.

Song, W., Wemheuer, B., Zhang, S., Steensen, K., Thomas, T., 2019. MetaCHIP: community-level horizontal gene transfer identification through the combination of best-match and phylogenetic approaches. Microbiome 7, 36.

Summers, A.O., Sugarman, L.I., 1974. Cell-free mercury(II)-reducing activity in a plasmid-bearing strain of Escherichia coli. J. Bacteriol. 119, 242–249.

Teelucksingh, T., Thompson, L.K., Cox, G., 2020. The evolutionary conservation of Escherichia coli drug efflux pumps supports physiological functions. J. Bacteriol. 202.

Uritskiy, G.V., DiRuggiero, J., Taylor, J., 2018. MetaWRAP-a flexible pipeline for genome-resolved metagenomic data analysis. Microbiome 6, 158.

Wales, A.D., Davies, R.H., 2015. Co-selection of resistance to antibiotics, biocides and heavy metals, and its relevance to foodborne pathogens. Antibiotics (Basel) 4, 567–604.

Xin, R., Banda, J.F., Hao, C., Dong, H., Pei, L., Guo, D., Wei, P., Du, Z., Zhang, Y., Dong, H., 2021. Contrasting seasonal variations of geochemistry and microbial community in two adjacent acid mine drainage lakes in Anhui Province,China. Environ. Pollut. 268, 115826.

Xu, S., Liu, Y., Wang, R., Zhang, T., Lu, W., 2022. Behaviors of antibiotic resistance genes (ARGs) and metal resistance genes (MRGs) during the pilot-scale biophysical drying treatment of sewage sludge: reduction of ARGs and enrichment of MRGs. Sci. Total Environ. 809, 152221.

Xue, C.X., Lin, H., Zhu, X.Y., Liu, J., Zhang, Y., Rowley, G., Todd, J.D., Li, M., Zhang, X.H., 2021. DiTing: a pipeline to infer and compare biogeochemical pathways from metagenomic and metatranscriptomic data. Front. Microbiol. 12, 698286.

Yi, X., Liang, J.L., Su, J.Q., Jia, P., Lu, J.L., Zheng, J., Wang, Z., Feng, S.W., Luo, Z.H., Ai, H.X., Liao, B., Shu, W.S., Li, J.T., Zhu, Y.G., 2022. Globally distributed mining-impacted environments are underexplored hotspots of multidrug resistance genes. ISME J. 16, 2099–2113.

Yin, X., Jiang, X.T., Chai, B., Li, L., Yang, Y., Cole, J.R., Tiedje, J.M., Zhang, T., 2018. ARGs-OAP v2.0 with an expanded SARG database and hidden markov models for enhancement characterization and quantification of antibiotic resistance genes in environmental metagenomes. Bioinformatics 34, 2263–2270.

Zagui, G.S., Moreira, N.C., Santos, D.V., Darini, A.L.C., Domingo, J.L., Segura-Muñoz, S.I., Andrade, L.N., 2021. High occurrence of heavy metal tolerance genes in bacteria isolated from wastewater: a new concern? Environ. Res. 196, 110352.

Zhao, R., Yu, K., Zhang, J., Zhang, G., Huang, J., Ma, L., Deng, C., Li, X., Li, B., 2020a. Deciphering the mobility and bacterial hosts of antibiotic resistance genes under antibiotic selection pressure by metagenomic assembly and binning approaches. Water Res. 186, 116318.

Zgurskaya, H.I., Malloci, G., Chandar, B., Vargiu, A.V., Ruggerone, P., 2021. Bacterial efflux transporters' polyspecificity - a gift and a curse? Curr. Opin. Microbiol. 61, 115–123.

Zhao, X., Shen, J.P., Zhang, L.M., Du, S., Hu, H.W., He, J.Z., 2020b. Arsenic and cadmium as predominant factors shaping the distribution patterns of antibiotic resistance genes in polluted paddy soils. J. Hazard. Mater. 389, 121838.

Zhuang, M., Achmon, Y., Cao, Y., Liang, X., Chen, L., Wang, H., Siame, B.A., Leung, K.Y., 2021. Distribution of antibiotic resistance genes in the environment. Environ. Pollut. 285, 117402.